The American Journal of Human Genetics, Volume *103*

Supplemental Data

MACF1 Mutations Encoding Highly Conserved Zinc-Binding Residues of the GAR Domain Cause Defects in Neuronal Migration and Axon Guidance

William B. Dobyns, Kimberly A. Aldinger, Gisele E. Ishak, Ghayda M. Mirzaa, Andrew E. Timms, Megan E. Grout, Marjolein H.G. Dremmen, Rachel Schot, Laura Vandervore, Marjon A. van Slegtenhorst, Martina Wilke, Esmee Kasteleijn, Arthur S. Lee, Brenda J. Barry, Katherine R. Chao, Krzysztof Szczałuba, Joyce Kobori, Andrea Hanson-Kahn, Jonathan A. Bernstein, Lucinda Carr, Felice D'Arco, Kaori Miyana, Tetsuya Okazaki, Yoshiaki Saito, Masayuki Sasaki, Soma Das, Marsha M. Wheeler, Michael J. Bamshad, Deborah A. Nickerson, University of Washington Center for Mendelian Genomics, Center for Mendelian Genomics at the Broad Institute of MIT and Harvard, Elizabeth C. Engle, Frans W. Verheijen, Dan Doherty, and Grazia M.S. Mancini

Figure S1

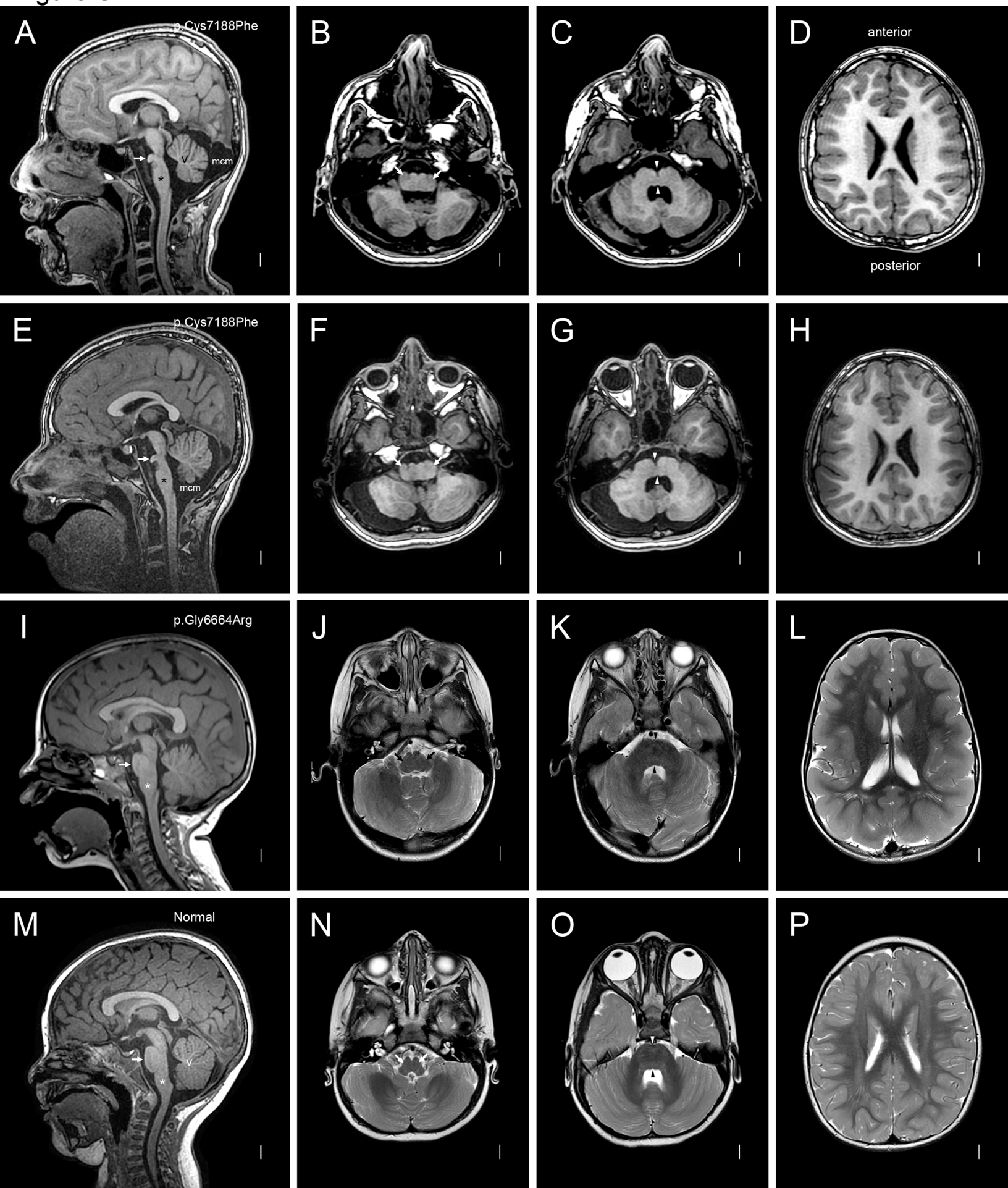
A
p.Cys7188Phe
V
mcm
*
B
C
D
anterior
posterior
E
p.Cys7188Phe
*
mcm
F
G
H
I
p.Gly6664Arg
*
J
K
L
M
Normal
V
*
N
O
P

Figure S1. Brain MRI with *MACF1* zinc-binding or rod domain mutations. Images from mid-sagittal (far left column) and three axial planes at the same levels as in Figure 1 are shown from subjects LR04-067a1 (A-D), LR04-067a2 (E-H), LR16-412 (I-L), and a normal control (M-P). *MACF1* mutations are shown in the far left column. Mid-sagittal images from the twins show striking brainstem dysplasia with mildly narrow midbrain, dramatically narrow pons with small but easily seen nodules on the ventral surface (arrows in A, E). The midline images also show borderline vermis hypoplasia (A, E). The medulla is very wide – almost double the typical width – with small pyramids visible on the ventral surface (white arrows in B, F). The pons is very narrow in the midline with a deep ventral cleft (arrowheads in C, G) but also very wide. Corresponding images in the girl with a mutation in the spectrum rod domain appear normal. Higher images in all three subjects including the girl with the rod domain mutation images show diffuse mild pachygyria (D, H) with a posterior more severe than anterior gradient, and only mildly thick cortex (also called “thin” LIS).

Figure S2

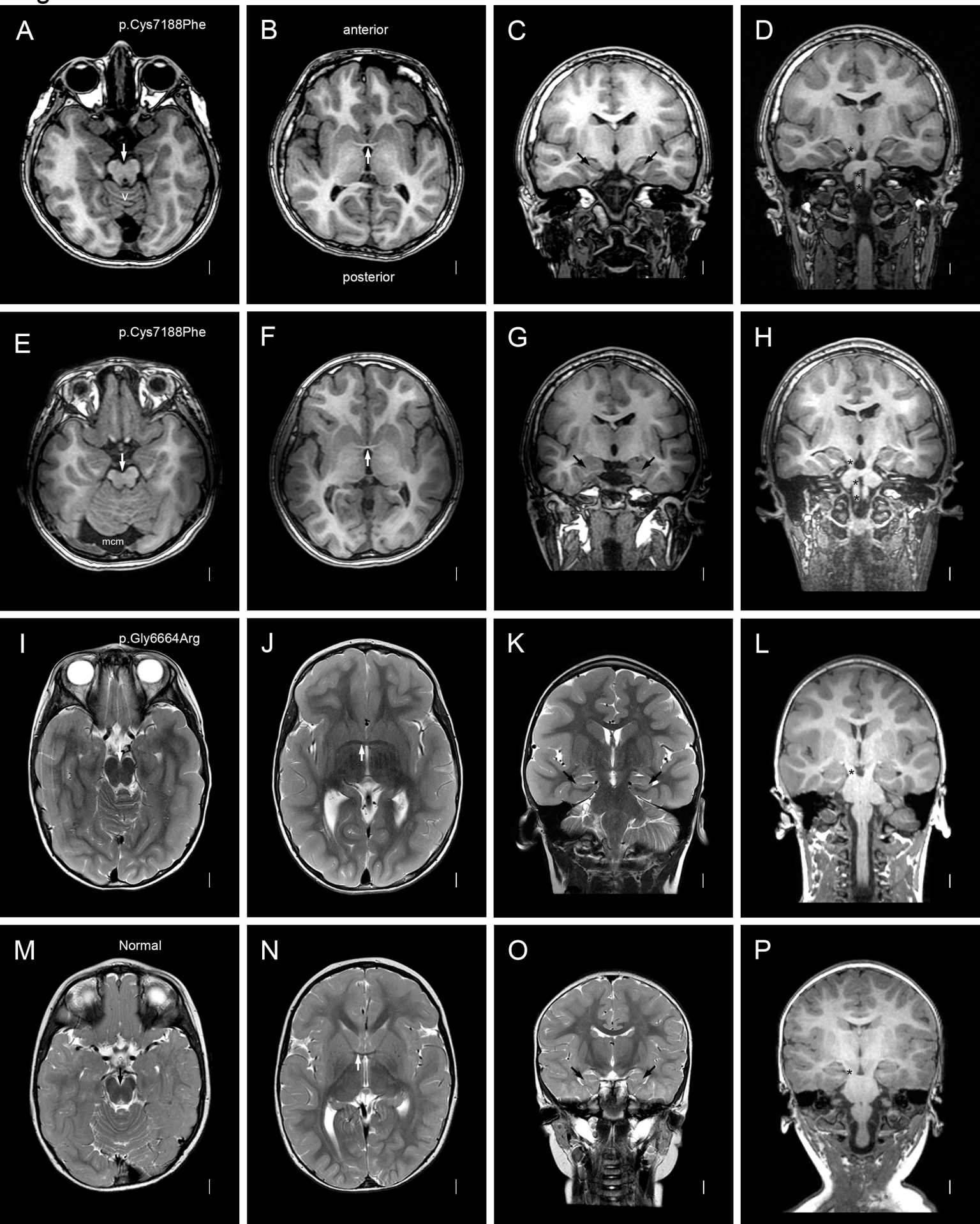
A
p.Cys7188Phe
v
B
anterior
posterior
C
D
E
p.Cys7188Phe
mcm
F
G
H
I
p.Gly6664Arg
J
K
L
M
Normal
N
O
P

Figure S2. Brain MRI with *MACF1* zinc-binding or rod domain mutations – additional features. Axial (left two columns), coronal (third column), and reconstructed coronal (far right column) images are shown for subjects LR04-067a1 (A-D), LR04-067a2 (E-H), LR16-412 (I-L), and a normal control (M-P). *MACF1* mutations are shown in the far left column. In the top two rows, the low midbrain appears mildly small with no features of the molar tooth malformation (A, E), the anterior commissures are very thin (arrows in B, F), and the hippocampi are small and dysplastic (C, G). The pyramidal tracts are easy to follow (asterisks over the right pyramidal tracts in D, H), although a small bundle of transverse pontine crossing fibers can be seen. Corresponding images for the girl with the rod domain mutation are normal except for borderline thick hippocampi (K). Mild pachygyria (thin LIS) can be seen on all of the axial and coronal images for the three patients (A-L).

Figure S3

A

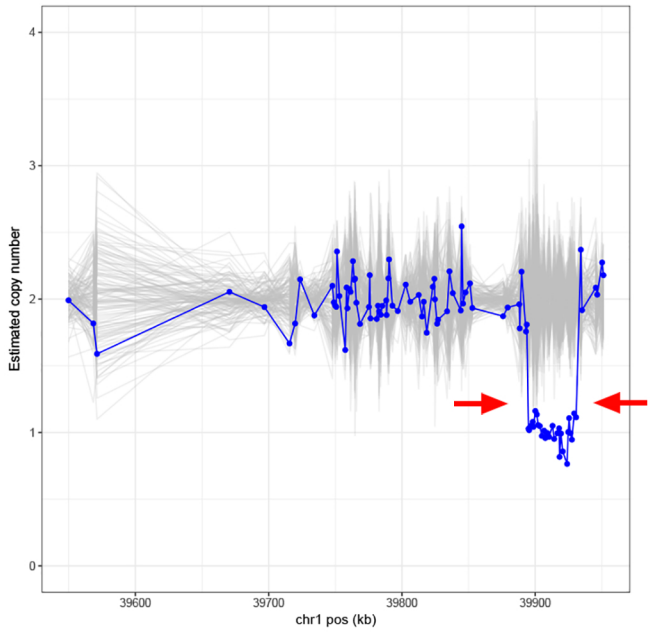

B

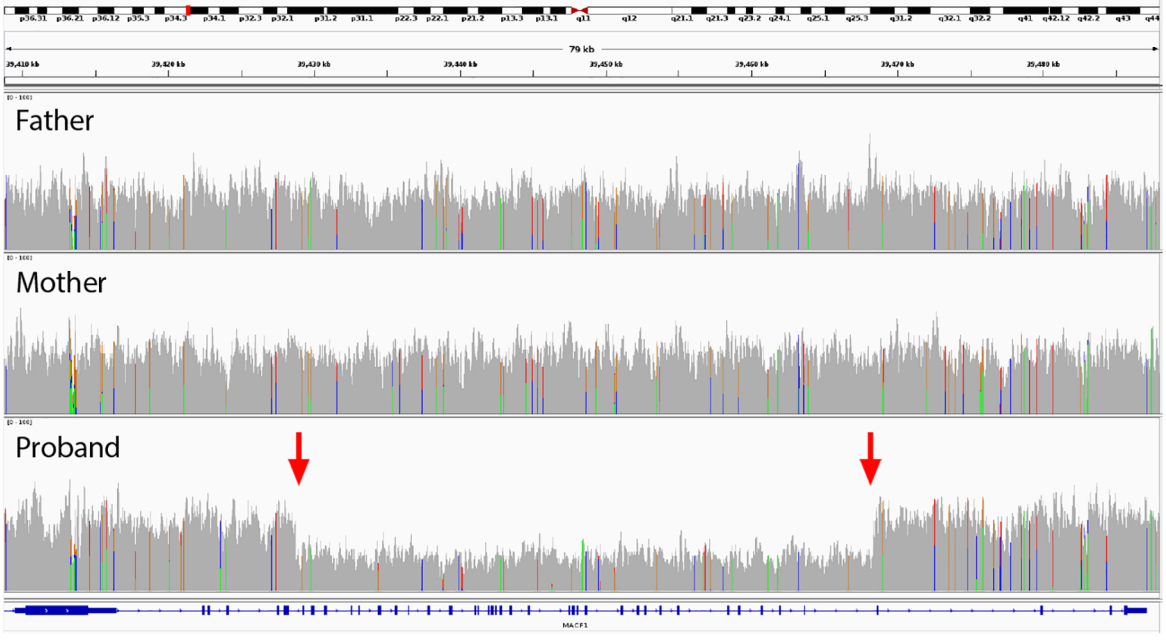

C

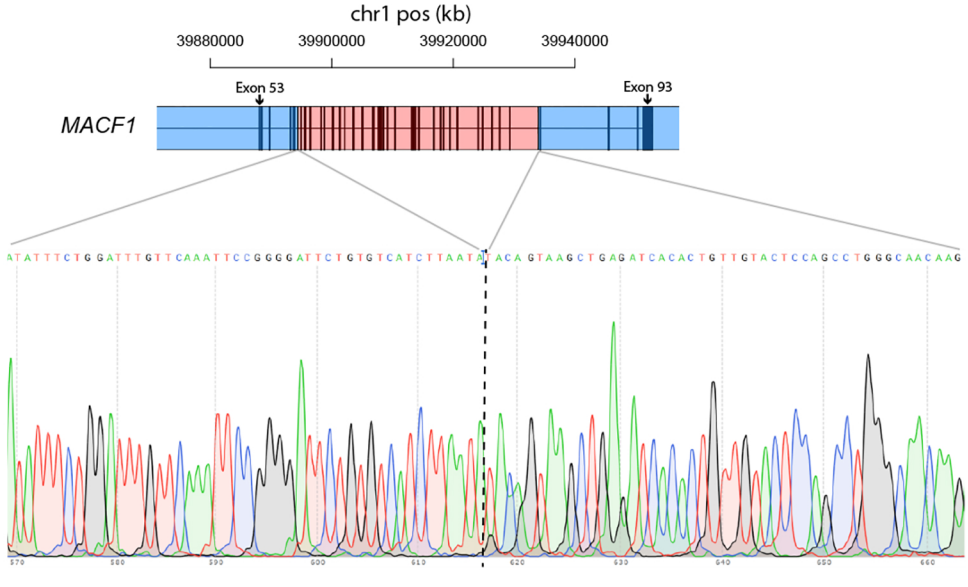

Figure S3. Molecular data supporting an intragenic deletion of *MACF1*. The top panel shows read depth (grey lines) and estimated copy number (blue lines) visualized with the GATK4 GermlineCNVCaller in subject LR18-070 (A). The obvious drop in estimated copy number from 2 to 1 seen just before the 5' end of the gene (red arrows in A) indicates a deletion. The deletion can also be seen in a screen shot from the Integrated Genome Viewer (IGV) using whole genome sequencing data (red arrows in B). A chromatogram from Sanger sequencing with primers on either side of the breakpoint validates location of the breakpoint (dashed vertical line in lower panel in C). Deleted sequence along the *MACF1* gene model (NM_012090.5) is shaded in red while flanking sequence is shaded in blue. Selected exon numbers are denoted by arrows.

Figure S4

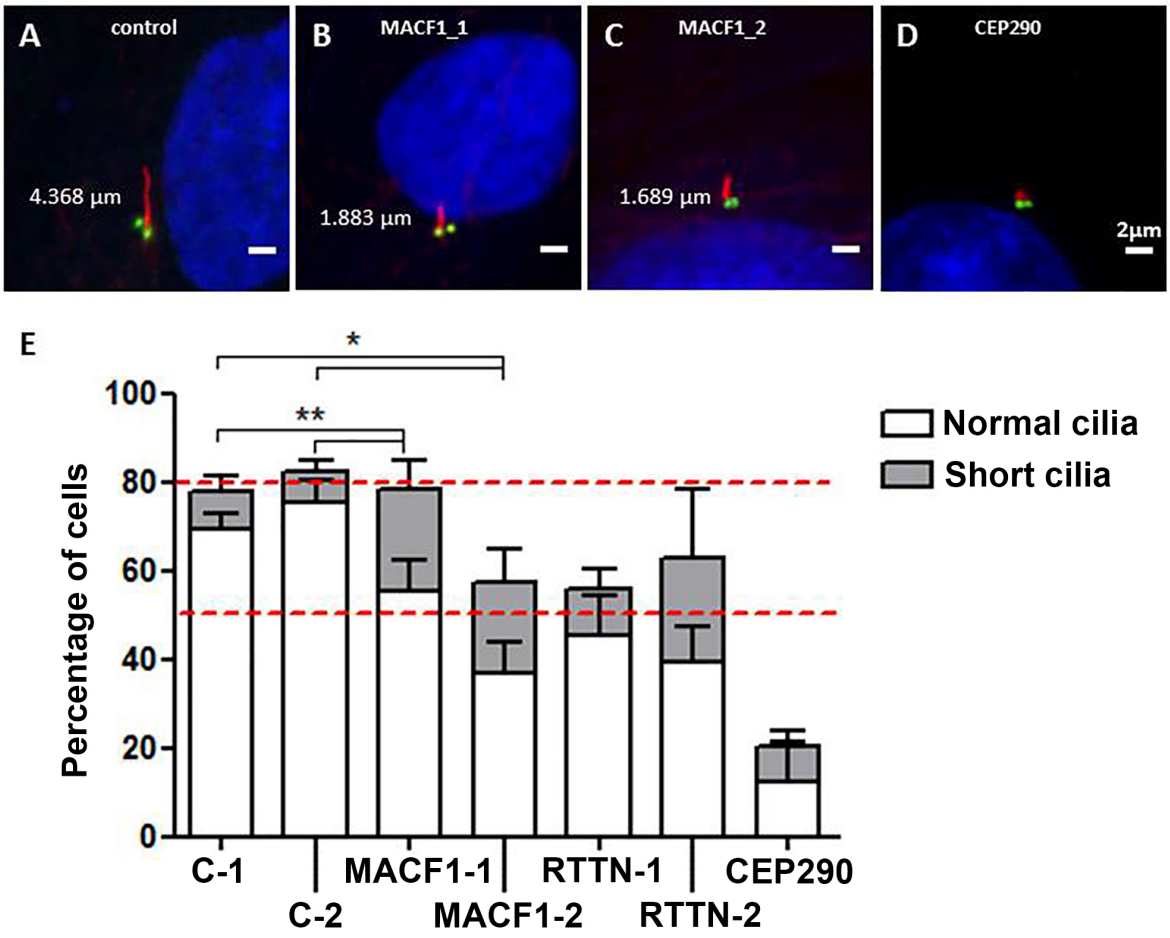

Figure S4. Cilia formation is abnormal with *MACF1* mutations. Formation of cilia was studied in cultured skin fibroblasts following serum starvation and immunostaining with antibodies against gamma-tubulin (basal bodies in green) and acetylated-tubulin (axoneme in red) by measuring both the proportion of cells with cilia and cilia length, with examples of normal (A), short (B, C) and absent (D) cilia shown. Experimental results are shown in a histogram (E) where the Y axis indicates the percentage of total cells in which the basal body has built a primary cilium, and the dark portion of the bars represent cells with an axoneme shorter than 3 µm. Results in two controls, two subjects with heterozygous *MACF1* mutations, two with biallelic *RTTN* mutations, and one with biallelic *CEP290* mutations (along the X axis) show a significant reduction in cilia length in subjects with mutations of *MACF1* or *RTTN*. In contrast, the subject with *CEP290* mutations has severely reduced cilia number. The normal range for ciliation rate (50-80%, dashed red lines) was determined from ~100 experiments using several different control fibroblast lines. Values indicate average plus standard error of the mean (SEM) for separate duplicate or quadruplicate experiments. While *Macf1*$^{-/-}$ mouse embryonic fibroblasts (MEFs) generate no cilia and *Macf1*$^{+/-}$ MEFs have normal cilia, we detect a significant ciliogenesis defect in humans with heterozygous *MACF1* mutation in the GAR domain (*p<0.01;

**p<0.001). The mutations include: MACF1-1 (LR17-434) and MACF1-2 (LR14-088), both heterozygous *MACF1*:p.Cys7135Phe de novo; RTTN-1, compound heterozygous *RTTN*:p.His865Arg and p.Glu1397Lysfs*7; RTTN-2, homozygous *RTTN*:p.Leu932Phe; and CEP290 compound heterozygous *CEP290*: p.Glu501* and p.Arg1508*.

Figure S5

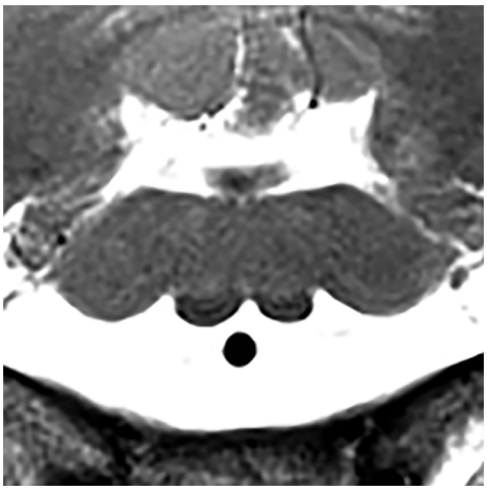

Figure S5. The brainstem malformation may resemble bird wings. Axial images through the medulla when inverted may resemble totem bird wings as shown here for subject LR14-088 (modified from Figure 1B). However, this has not been consistent enough to justify common use.

Table S1. Whole exome and genome sequencing parameters

	LIS with brainstem hypoplasia-dysplasia				
Subject	LR14-088	LR17-434	LR16-306	LR17-450	LR04-067a2
Mutation (MACF1-204)	p.Cys7135Phe	p.Cys7135Phe	p.Asp7186Tyr	p.Asp7186Tyr	p.Cys7188Phe
Testing basis	Research	Clinical	Clinical	Research	Clinical
Testing center	Illumina	ErasmusMC	Baylor	UWCMG	UCGSL
Testing approach	Trio	Trio	Proband	Trio	Trio
NGS type	Exome/Genome	Exome	Exome	Exome	Exome
Capture	NA	SureSelect CRE	SeqCap EZ	Nimblegen_v2	SureSelect
Total reads	997488792	36857470	110212766	60070882	195502268
Total aligned reads (%)	982449620 (98.49%)	36809635 (99,9%)	110099130 (99.90%)	59945462 (99.79%)	192651214 (98.54%)
Median read length	150	150	101	75	150
Mean coverage	46.05	50.05	154.73	53.08	195.35
5X	99.92	97.7	99.42	98.70	97.50%
10X	99.91	96	99.28	96.50	97.30%
20X	99.84	90.4	98.82	88.50	96.50%
50X	33.73	64.8	91.02	47.10	92.50%
Reference for methods	1	2	5	6	4

Abbreviations: NA, not applicable; SureSelect, Illumina SureSelect®; UCGSL, University of Chicago Genetic Services Laboratories; UWCMG, University of Washington Center for Mendelian Genomics. Only Sanger sequencing was performed in subjects LR04-067a1 (twin) and LR18-077.

Table S1, continued

	LIS-brainstem	LIS only
Subject	LR18-070[13]	LR16-412
Mutation (MACF1-204)	Deletion	p.Gly6664Arg
Testing basis	Research	Clinical
Testing center	Broad Institute	GeneDx
Testing approach	Trio	Trio
NGS type	Exome/Genome	Exome
Capture	SureSelect	SureSelect HAE
Total reads	196860614	54873093
Total aligned reads (%)	195183707 (99.1%)	54721312 (99.72%)
Median read length	101	150
Mean coverage	144.98	123.22
5X	NA	98.81
10X	90.37	98.66
20X	88.08	98.10
50X	79.51	91.78
Reference for methods	7	17

Table S2. *MACF1* mutation and protein variant data

					Transcript NM_012090.5[a]	
Subject ID	**Chr**	**Position [hg19]**	**Ref**	**Alt**	**cDNA**	**Protein**
LIS-BSH						
LR14-088	1	g.39929312	G	T	c.15530G>T	p.Cys5177Phe
LR17-434	1	g.39929312	G	T	c.15530G>T	p.Cys5177Phe
LR16-306	1	g.39934392	G	T	c.15682G>T	p.Asp5228Tyr
LR17-450	1	g.39934392	G	T	c.15682G>T	p.Asp5228Tyr
LR18-077	1	g.39934398	T	G	c.15688T>G	p.Cys5230Gly
LR04-067a1[f]	1	g.39934399	G	T	c.15689G>T	p.Cys5230Phe
LR04-067a2[f]	1	g.39934399	G	T	c.15689G>T	p.Cys5230Phe
LR18-070[13]	1	g.39894403[g]	39.6 kb deletion		exon 58-89 deletion[h]	p.Ala3540_Arg5192del
LIS only						
LR16-412	1	g.39916758	G	C	c.14116G>C	p.Gly4706Arg
SCZ only						
Kenny 2014[14]	1	g.39788292[i]	CAAC	TA	c.4057_4060delinsTA	p.Gln1353Tyrfs*55
Wang 2015[15]	1	g.39827053	C	T	c.6289C>T	p.Arg2097Trp
Xu 2012[16]	1	g.39904999	C	T	c.12097C>T	p.Arg4033Trp

Table S2. continued

	Transcript MACF1-204[b]				
Subject ID	**cDNA**	**Protein**	**Mutation type[c]**	**CADD[d]**	**PolyPhen-2[e]**
LIS-BSH					
LR14-088	c.21404G>T	p.Cys7135Phe	Missense	34	0.997[j]
LR17-434	c.21404G>T	p.Cys7135Phe	Missense	34	0.997[j]
LR16-306	c.21556G>T	p.Asp7186Tyr	Missense	34	0.999[j]
LR17-450	c.21556G>T	p.Asp7186Tyr	Missense	34	0.999[j]
LR18-077	c.21562T>G	p.Cys7188Gly	Missense	31	0.995[j]
LR04-067a1[d]	c.21563G>T	p.Cys7188Phe	Missense	34	0.997[j]
LR04-067a2[d]	c.21563G>T	p.Cys7188Phe	Missense	34	0.997[j]
LR18-070[13]	exon 62-93 deletion	p.Ala5498_Arg7150del	Deletion (in frame)	NA	--
LIS only					
LR16-412	c.19990G>C	p.Gly6664Arg	Missense	34	0.999[j]
SCZ only					
Kenny 2014[14]	c.4057_4060delinsTA	p.Gln1353Tyrfs*55	Indel	36	--
Wang 2015[15]	c.12490C>T	p.Arg4164Trp	Missense	25	0.022[k]
Xu 2012[16]	c.17971C>T	p.Arg5991Trp	Missense	34	0.993[j]

Abbreviations: Alt, alternate allele; Chr, chromosome; LIS, lissencephaly; NA, not applicable; Ref, reference allele; SCZ, schizophrenia. Footnotes: [a]NCBI Reference Sequence NM_012090.5 and Ensemble Sequence MACF1-203, transcript ID ENST00000361689.6; [b]Ensemble Sequence MACF1-204, transcript ID ENST00000372915.7; [c]Variants were all de novo; [d]CADD version 1.3 (http://cadd.gs.washington.edu/home); [e]Variants were all Not Scored by SIFT; [f]monozygotic twins; [g]g.39894403_39934001del; [h]c.10617+444_15577-288del; [i]g.39788292_39788295delinsTA; [j]probably damaging; [k]benign.

SUPPLEMENTAL METHODS

Participants

Clincal data including brain imaging studies performed as part of routine care were reviewed and summarized (Tables 1-2). Skin biopsies were performed on two children and used to establish fibroblast cultures by standard methods.

Molecular methods

Whole exome and genome sequencing were performed at seven different centers using center specific pipelines as described previously (Table S1).[1-7] The small intragenic deletion found in subject LR18-070 was confirmed in whole genome data using the Manta SV caller,[8] and in whole exome data using the GATK4 GermlineCNVCaller (Box 1).[9] We designed primers flanking the breakpoint (forward primer: CAGGCCCGATACAGTGAAAT; and reverse primer: AACAGACAGACCCCACCATC), and performed PCR under the following conditions: 95°C for 1 min. followed by 35 cycles of 94°C for 10 seconds, 60°C for 10 seconds, and 72°C for 1 second. Sanger sequencing was then performed using these primers.

Protein modeling

The solved structure of the human MACF1 (a.k.a. hACF7) EF1-EF2-GAR domains (5VE9.pdb in the RCSB Protein Data Bank) was loaded in PyMOL Molecular Graphics System (version 1.5.0.5, Schrödinger, LLC).[10; 11] The wild type Cys-Cys-Asp-Cys residues and coordinated zinc ion were visualized as stick models. Simulations of four missense variants in the GAR domain were computed using the PyMOL mutagenesis wizard.

Cilia number and length in cultured fibroblasts

Skin-derived fibroblast cell lines from two control individuals and five subjects with mutations of *MACF1* or two other genes (*RELN*, *CEP290*) known to regulate cilia formation were grown and processed in parallel in duplicate or quadruplicate as previously described.[12]

Immunocytochemisty. Fibroblasts were plated at $5x10^4$ cells/cm^2 on 24 mm cover slips (Thermo Fisher Scientific®), and cultured in 2 mL DMEM+/+ (10% Fetal Calf Serum, 1% PenStrep, Lonza®) in a 6 well plate. The next day, cell confluency reached 80% and culture media was replaced with 2mL DMEM-/-. Cells were serum starved for 48 hours to induce ciliogenesis. After fixing cells with methanol for 10 minutes at -20 °C, coverslips were incubated with blocking buffer containing 50mM Tris HCl pH 7.4, 0.9% NaCl, 0.25% gelatin, and 0.5% TritonX-100 for 10 minutes on ice. Primary and secondary antibody dilutions were prepared in blocking buffer. Incubation with primary antibody was done overnight at 4°C. Slips were washed with 1x PBS (Sigma Aldrich®) and incubated with secondary antibody for 1 hour at room temperature. After washing, coverslips were placed on a microscope slide with 20 µL ProLong® Gold Antifade Reagent with DAPI (Thermo Fisher Scientific®) and dried in 37 °C for 4 hours.

Antibodies. Primary antibodies used included mouse monoclonal anti-human acetylated tubulin (Sigma Aldrich® T7451), and rabbit polyclonal anti-human gamma tubulin (Sigma Aldrich® T3320). The secondary antibodies used in a 1 in 10,000 dilution were Green DyLight TM488-

conjugated AffiniPure Donkey Anti-Rabbit IgG, and Red Cy™3 AffiniPure Donkey Anti-Mouse IgG (H+L)(Jackson Laboratories® 715-165-150).

Experimental design. Cells from five individuals with known mutations (*MACF1* x2, *RTTN* x2, *CEP290* x1) and two control lines – were processed in parallel in duplicate or quadruplicate as previously described.[12] Dishes were blinded, and cells with basal bodies (γ-tubulin-positive) were scored for cilia length, defined as normal (>3 μm) or short (<3 μm), in four different quadrants for each coverslip by one individual. Values indicate average +/- SEM. Under these conditions, 50-80% of cells grow cilia based on data from 100 experiments using multiple control fibroblast lines. Statistical tests were performed using Prism 5 GraphPad.

WEB RESOURCES

GATK4 GermlineCNVCaller
<https://github.com/broadinstitute/gatk/tree/master/scripts/cnv_wdl/germline>
Manta Structural Variant Caller
<https://github.com/Illumina/manta>

SUPPLEMENTARY REFERENCES

1. Alcantara, D., Timms, A.E., Gripp, K., Baker, L., Park, K., Collins, S., Cheng, C., Stewart, F., Mehta, S.G., Saggar, A., et al. (2017). Mutations of AKT3 are associated with a wide spectrum of developmental disorders including extreme megalencephaly. Brain 140, 2610-2622.
2. Oegema, R., Baillat, D., Schot, R., van Unen, L.M., Brooks, A., Kia, S.K., Hoogeboom, A.J.M., Xia, Z., Li, W., Cesaroni, M., et al. (2017). Human mutations in integrator complex subunits link transcriptome integrity to brain development. PLoS Genet 13, e1006809.
3. Di Gioia, S.A., Connors, S., Matsunami, N., Cannavino, J., Rose, M.F., Gilette, N.M., Artoni, P., de Macena Sobreira, N.L., Chan, W.M., Webb, B.D., et al. (2017). A defect in myoblast fusion underlies Carey-Fineman-Ziter syndrome. Nat Commun 8, 16077.
4. Sun, M., Knight Johnson, A., Nelakuditi, V., Guidugli, L., Fischer, D., Arndt, K., Ma, L., Sandford, E., Shakkottai, V., Boycott, K., et al. (2018 in press). Exome sequencing and targeted analysis identifies the genetic basis of disease in over 50% of patients with a wide range of ataxia-related phenotypes. Genet Med.
5. Yang, Y., Muzny, D.M., Reid, J.G., Bainbridge, M.N., Willis, A., Ward, P.A., Braxton, A., Beuten, J., Xia, F., Niu, Z., et al. (2013). Clinical Whole-Exome Sequencing for the Diagnosis of Mendelian Disorders. N Engl J Med.
6. Van De Weghe, J.C., Rusterholz, T.D.S., Latour, B., Grout, M.E., Aldinger, K.A., Shaheen, R., Dempsey, J.C., Maddirevula, S., Cheng, Y.H., Phelps, I.G., et al. (2017). Mutations in ARMC9, which Encodes a Basal Body Protein, Cause Joubert Syndrome in Humans and Ciliopathy Phenotypes in Zebrafish. Am J Hum Genet 101, 23-36.

7. Poulsen, J.B., Lescai, F., Grove, J., Baekvad-Hansen, M., Christiansen, M., Hagen, C.M., Maller, J., Stevens, C., Li, S., Li, Q., et al. (2016). High-Quality Exome Sequencing of Whole-Genome Amplified Neonatal Dried Blood Spot DNA. PLoS One 11, e0153253.
8. Chen, X., Schulz-Trieglaff, O., Shaw, R., Barnes, B., Schlesinger, F., Kallberg, M., Cox, A.J., Kruglyak, S., and Saunders, C.T. (2016). Manta: rapid detection of structural variants and indels for germline and cancer sequencing applications. Bioinformatics 32, 1220-1222.
9. McKenna, A., Hanna, M., Banks, E., Sivachenko, A., Cibulskis, K., Kernytsky, A., Garimella, K., Altshuler, D., Gabriel, S., Daly, M., et al. (2010). The Genome Analysis Toolkit: a MapReduce framework for analyzing next-generation DNA sequencing data. Genome Res 20, 1297-1303.
10. Alexander, N., Woetzel, N., and Meiler, J. (2011). bcl::Cluster: A method for clustering biological molecules coupled with visualization in the Pymol Molecular Graphics System. IEEE Int Conf Comput Adv Bio Med Sci 2011, 13-18.
11. Lane, T.R., Fuchs, E., and Slep, K.C. (2017). Structure of the ACF7 EF-Hand-GAR Module and Delineation of Microtubule Binding Determinants. Structure 25, 1130-1138 e1136.
12. Kheradmand Kia, S., Verbeek, E., Engelen, E., Schot, R., Poot, R.A., de Coo, I.F., Lequin, M.H., Poulton, C.J., Pourfarzad, F., Grosveld, F.G., et al. (2012). RTTN mutations link primary cilia dunction to organization of the human cerebral cortex. Am J Hum Genet 91, 533-540.
13. Irahara, K., Saito, Y., Sugai, K., Nakagawa, E., Saito, T., Komaki, H., Nakata, Y., Sato, N., Baba, K., Yamamoto, T., et al. (2014). Pontine malformation, undecussated pyramidal tracts, and regional polymicrogyria: a new syndrome. Pediatr Neurol 50, 384-388.
14. Kenny, E.M., Cormican, P., Furlong, S., Heron, E., Kenny, G., Fahey, C., Kelleher, E., Ennis, S., Tropea, D., Anney, R., et al. (2014). Excess of rare novel loss-of-function variants in synaptic genes in schizophrenia and autism spectrum disorders. Mol Psychiatry 19, 872-879.
15. Wang, Q., Li, M., Yang, Z., Hu, X., Wu, H.M., Ni, P., Ren, H., Deng, W., Li, M., Ma, X., et al. (2015). Increased co-expression of genes harboring the damaging de novo mutations in Chinese schizophrenic patients during prenatal development. Sci Rep 5, 18209.
16. Xu, B., Ionita-Laza, I., Roos, J.L., Boone, B., Woodrick, S., Sun, Y., Levy, S., Gogos, J.A., and Karayiorgou, M. (2012). De novo gene mutations highlight patterns of genetic and neural complexity in schizophrenia. Nat Genet 44, 1365-1369.
17. Retterer, K., Juusola, J., Cho, M.T., Vitazka, P., Millan, F., Gibellini, F., Vertino-Bell, A., Smaoui, N., Neidich, J., Monaghan, K.G., et al. (2016). Clinical application of whole-exome sequencing across clinical indications. Genet Med 18, 696-704.